

TECHNICAL NOTE

Imaging of Hypoxic Tumor: Correlation between Diffusion-weighted MR Imaging and ¹⁸F-fluoroazomycin Arabinoside Positron Emission Tomography in Head and Neck Carcinoma

Akiko Imaizumi^{1*}, Takayuki Obata¹, Jeff Kershaw¹, Yasuhiko Tachibana¹, Masayuki Inubushi², Mitsuru Koizumi³, Kyosan Yoshikawa⁴, Ming-Rong Zhang⁵, Katsuyuki Tanimoto⁶, Rintaro Harada⁷, Takashi Uno⁷, and Tsuneo Saga⁸

We investigated the usefulness of diffusion-weighted imaging (DWI) for detecting changes in the structure of hypoxic cells by evaluating the correlation between ¹⁸F-fluoroazomycin arabinoside (FAZA) positron emission tomography activity and DWI parameters in head and neck carcinoma. The diffusion coefficient corresponding to the slow compartment of a two-compartment model had a significant positive correlation with FAZA activity ($\rho = 0.58$, $P = 0.016$), whereas the diffusional kurtosis from diffusion kurtosis imaging had a significant negative correlation ($\rho = -0.62$, $P = 0.008$), which suggests that those DWI parameters might be useful as indicators for changes in cell structure.

Keywords: *diffusion-weighted imaging, ¹⁸F-fluoroazomycin arabinoside positron emission tomography, head and neck carcinoma, hypoxia*

Introduction

Hypoxic tumors are highly malignant and frequently develop invasive growths and metastasis. They are also highly resistant to radiotherapy and chemotherapy.¹ If the hypoxic condition of the tumor could be precisely assessed, it is expected that such a measurement would be useful for

predicting therapeutic effects and selecting suitable treatments. Moreover, if the hypoxic area within the tumor can be identified, hypoxia-targeting therapy would be feasible. ¹⁸F-fluoromisonidazole (FMISO) and ¹⁸F-fluoroazomycin arabinoside (FAZA)-positron emission tomography (PET) have been reported to be useful for non-invasive hypoxic imaging, but they are not commonly available in clinical practice.^{2–4} The hypoxic area of the tumor exists between the normoxic and necrotic areas.¹ In hypoxic tissue, an increase of cell membrane permeability and cell diameter, and destruction of cell membrane have been reported.⁵ Changes in cell structure caused by hypoxia lead to alterations in water diffusion, and it is possible that this can be detected on diffusion-weighted imaging (DWI) and MRI.⁶

The most commonly used quantity obtained from DWI is the apparent diffusion coefficient (ADC), which characterizes mono-exponential decay of the signal. However, because water diffusion in biological tissue is complex, the tissue structure cannot be fully described by the ADC alone. This is because the ADC model assumes that the diffusion of water molecules is Gaussian, however, it is well known that *in vivo* diffusion is non-Gaussian due to the restriction of molecular motion by the complex microstructure. In particular, this is observed at high *b*-values when the signal change deviates from mono-exponential decay. Alternatively, the signal is often modeled with a bi-exponential equation corresponding to a two-compartment model. In this model, the water diffusion is

¹Applied MRI Research, Molecular Imaging and Theranostics, National Institute of Radiological Sciences, National Institutes for Quantum and Radiological Science and Technology, 4-9-1 Anagawa, Inage-ku, Chiba, Chiba 263-8555, Japan

²Division of Nuclear Medicine, Department of Radiology, Kawasaki Medical School, Okayama, Japan

³Department of Nuclear Medicine, Cancer Institute Hospital, Japanese Foundation for Cancer Research, Tokyo, Japan

⁴Advanced Imaging Center, Tokyo Bay Advanced Imaging and Radiation Oncology Clinic Makuhashi, Aoiikai Medical Corporation, Chiba, Japan

⁵Department of Radiopharmaceuticals Development, National Institute of Radiological Sciences, National Institutes for Quantum and Radiological Science and Technology, Chiba, Japan

⁶Hospital of the National Institute of Radiological Sciences, National Institutes for Quantum and Radiological Science and Technology, Chiba, Japan

⁷Diagnostic Radiology and Radiation Oncology, Graduate School of Medicine, Chiba University, Chiba, Japan

⁸Department of Diagnostic Imaging and Nuclear Medicine, Graduate School of Medicine, Kyoto University, Kyoto, Japan

*Corresponding author, Phone: +81-43-206-3230, Fax: +81-43-251-4531, E-mail: aima.izumi13@gmail.com

©2019 Japanese Society for Magnetic Resonance in Medicine

This work is licensed under a Creative Commons Attribution-NonCommercial-NoDerivatives International License.

Received: January 23, 2019 | Accepted: August 3, 2019

divided into fast and slow compartments.⁷ The slow compartment corresponds to intracellular water molecules, where diffusion of the water molecules is restricted by intracellular structure and cell membrane. Therefore, changes in the cell structure might be estimated with the two-compartment model.⁷ Another way to interpret non-mono-exponential signal decay is the diffusion kurtosis model.⁸ In diffusion kurtosis imaging (DKI), the diffusional kurtosis (K), which is a parameter quantifying the degree of deviation from Gaussian behavior, is obtained. It has been reported that K increases under increased complexity of the tissue and increased restriction of the water diffusion.⁸

The purpose of this study was to investigate the usefulness of DWI for detecting changes in the structure of hypoxic cells by evaluating the correlation between FAZA-PET activity and several DWI parameters in head and neck carcinoma. To the best of our knowledge, this is the first study to perform an analysis of this type for head and neck carcinoma.

Materials and Methods

Subjects

This study was conducted with the approval of the Institutional Review Board, and written informed consent was obtained from all patients. From 32 patients enrolled in a previous FAZA study, the 11 patients who also underwent DWI were selected for this study.³ All patients were histopathologically diagnosed with head and neck carcinoma after biopsy. None of the patients had undergone any form of

treatment before DWI and FAZA-PET. Cases where a lesion could not be detected on DW images due to severe magnetic susceptibility artifact or motion artifact were excluded. Metastatic lymph nodes that showed necrotic change on T_1 - and T_2 -weighted images were also excluded. Nine primary tumors and eight metastatic lymph nodes without necrosis were evaluated. Patient data is summarized in Table 1. FAZA-PET and DWI were performed on the same day in 10 cases, and DWI was performed 1 day after FAZA-PET in one case.

DWI acquisition

DWI was performed using a 3T system (Magnetom Verio; Siemens, Erlangen, Germany). The echo planar imaging sequence was used with the following imaging parameters: TR 5000 ms, TE 98 or 105 ms, and b -value increased from 0 to 3000 s/mm^2 in 16 steps. Other parameters are summarized in Table 2. Images were acquired at a level where the lesion showed a maximum diameter on the image. Also, T_1 - and T_2 -weighted imaging were performed, and the imaging parameters are summarized in Table 2.

DWI analysis

Estimates for the parameters of each DWI model (ADC, two-compartment, DKI) were separately obtained for each lesion.

For the two-compartment model, two diffusion coefficients (D_f , D_s) and the volume fractions of the fast (F_f) and slow (F_s) compartments were estimated (note that $F_f + F_s = 1$). The signal change was fitted as a function of b -value to the following bi-exponential equation using the non-linear least squares method (Equations [1]).

Table 1 Summary of the 11 patients with head and neck carcinoma

No.	Age/Sex	Histopathology	Location of primary tumor	Primary tumor or metastatic lymph node	Tumor size (mm ²)
1	65/M	Squamous cell Ca	Oropharynx	mLN	36 × 24
2	63/F	Squamous cell Ca	Oropharynx	PT	18 × 18
				mLN	11 × 11
3	53/M	Squamous cell Ca	Oropharynx	PT	61 × 37
4	64/M	Squamous cell Ca	Oropharynx	PT	44 × 28
5	67/M	Squamous cell Ca	Oropharynx	PT	45 × 31
				mLN	16 × 15
6	76/M	Squamous cell Ca	Oral cavity	PT	38 × 23
				mLN	9 × 8
7	52/M	Squamous cell Ca	Paranasal sinus	PT	39 × 17
8	71/M	Squamous cell Ca	Hypopharynx	PT	16 × 13
9	64/M	Cylindrical cell Ca	Nasal cavity	PT	63 × 19
				mLN	11 × 10
				mLN	20 × 19
10	58/M	Undifferentiated Ca	Epipharynx	PT	31 × 31
11	51/M	Lymphoepithelial Ca	Epipharynx	mLN	25 × 17

Ca, carcinoma; mLN, metastatic lymph node; PT, primary tumor.

Table 2 Imaging parameters

	DWI	T ₁ - weighted imaging	T ₂ - weighted imaging
<i>b</i> -value (s/mm ²)	0, 50, 100, 200, 300, 500, 700, 900, 1100, 1300, 1500, 1700, 2000, 2300, 2600, 3000		
TR (ms)	5000	501–678	5500
TE (ms)	98/105	12	85
BW (Hz/pixel)	1184/1202	252	240
Number of averages	1	1	1
Slice thickness (mm)	5	3	3
FOV (mm ²)	220 × 220	180 × 180/200 × 200	180 × 180/200 × 200
Matrix size	112 × 160/128 × 128	224 × 320	224 × 320

BW, bandwidth; DWI, diffusion-weighted imaging.

$$S(b) = S_0 (F_f e^{-bD_f} + F_s e^{-bD_s}) \quad [1]$$

$S(b)$, S_0 : the signals with and without motion probing gradient (MPG), b : b -value.

The ADC was separately obtained using mono-exponential fitting for low (0–900 s/mm², ADC_{LB}) and high (1500–3000 s/mm², ADC_{HB}) b -value ranges (Equations [2] and [3]).
 $0 \leq b \leq 900$ s/mm²:

$$S(b) = S_{0,LB} e^{-bADC_{LB}} \quad [2]$$

$1500 \leq b \leq 3000$ s/mm²:

$$S(b) = S_{0,HB} e^{-bADC_{HB}} \quad [3]$$

$S_{0,LB}$: the signal without an applied MPG for the low b -value range, $S_{0,HB}$: the signal without an applied MPG for the high b -value range.

Images with b -values from 200 to 2000 s/mm² were used for DKI analysis. Outside of this range, the low b -value images were not used to eliminate the effect of intravoxel incoherent motion, and high b -value images were not used to improve the precision of the fitting.^{9,10} Signals were fitted to the following quadratic equation, and estimates of the diffusional kurtosis (K) and corrected diffusion coefficient (D) were obtained pixel-by-pixel (Equation [4]).

$$S(b) = S_0 e^{\left(-bD + \frac{1}{6}b^2D^2K\right)} \quad [4]$$

A region of interest (ROI) was manually drawn on each lesion while referring to the T₁- and T₂-weighted images. The

median values of the parameter estimates inside the ROI were used for statistical analysis. The median value was used instead of the mean value to reduce the influence of outlying values in the ROI. The mean ROI size was 378 mm² (range 56–830 mm²).

FAZA-PET acquisition

PET scanning was started 2 h after intravenous administration of FAZA (mean 374 ± 31 MBq). PET–CT scanning was performed using either an Aquiduo (Toshiba Medical Systems, Tochigi, Japan) or Biograph 16 (Siemens). An ROI was drawn on the lesion, and the maximum standardized uptake value (SUV_{max}) was measured. ROIs were also placed on the muscles at the back of the neck on both sides at the level of the hyoid bone, and the average SUV (SUV_{mean}) was obtained. The tumor-to-muscle ratio (T/M) was then calculated by dividing the lesion SUV_{max} by the muscle SUV_{mean}.³

Statistical analysis

Statistical analyses were performed with MATLAB version R2015a (MathWorks Inc., Natick, MA, USA). The Mann–Whitney U -test was used to compare the values of the DWI parameter estimates and FAZA-PET T/M between the primary tumors and the metastatic lymph nodes. Correlations between the DWI parameter estimates and the T/M were evaluated using Spearman's rank correlation coefficient. $P < 0.05$ was considered to be statistically significant.

Results

The primary tumor of a representative case (patient no. 5) is shown on both DWI and FAZA-PET in Fig. 1.

There was no statistically significant difference between the parameter estimates for the primary tumors and those for the metastatic lymph nodes (Table 3). Therefore, in the following analysis the primary tumors and the metastatic lymph nodes were analyzed together.

A significant positive correlation between D_s and T/M ($\rho = 0.58$, $P = 0.016$), and a significant negative correlation between K and T/M ($\rho = -0.62$, $P = 0.008$) were obtained (Fig. 2). There was no statistically significant correlation between the other DWI estimates and the T/M (Table 4).

Discussion

The usefulness of FAZA has been reported for head and neck, lung, and rectal cancers.^{3,4} Good agreement was found when FAZA accumulation was compared with the distribution of other hypoxic markers, and FAZA accumulation was higher in lower oxygenated tissue.¹¹

In the two-compartment model, the slow compartment is thought to reflect the diffusion of intracellular water molecules. Therefore, it is expected that increase of the cell membrane permeability, increase of the cell diameter, and

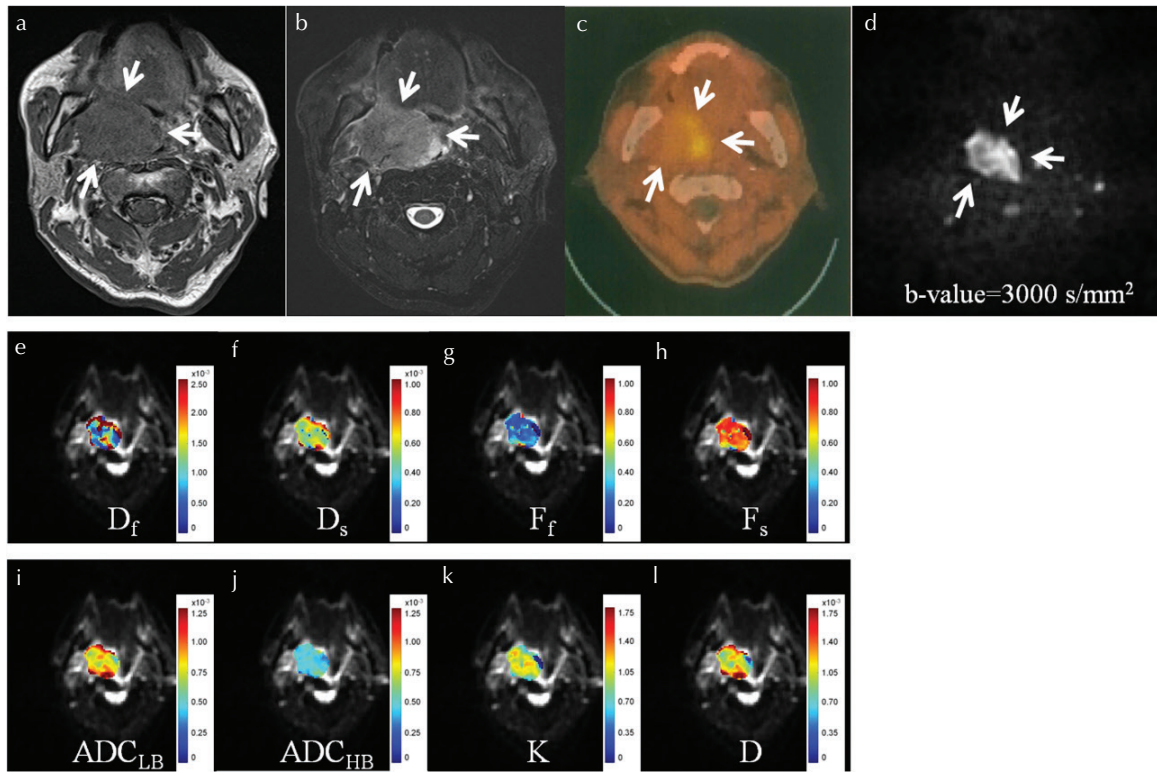


Fig. 1 A 67-year-old male patient with right oropharyngeal squamous cell carcinoma (patient no. 5). Conventional MR images demonstrate a tumor mass (arrows) with inhomogeneous intermediate signal intensity on the T₁-weighted image (a) and high signal intensity on the T₂-weighted image (b). Inhomogeneous ¹⁸F-fluoroazomycin arabinoside (FAZA) uptake is also seen on the FAZA-positron emission tomography/computed tomography image (c). The tumor-to-muscle ratio (T/M) was 3.21. A tumor mass is clearly delineated on the diffusion-weighted (DW) image acquired with b -value 3000 s/mm² (d). Color maps of the DW imaging parameter estimates are superimposed on the $b = 0$ s/mm² image (e–l). The median value was 2.07×10^{-3} mm²/s for D_f (e), 0.52×10^{-3} mm²/s for D_s (f), 0.25 for F_f (g), 0.75 for F_s (h), 0.77×10^{-3} mm²/s for ADC_{LB} (i), 0.45×10^{-3} mm²/s for ADC_{HB} (j), 0.60 for K (k), and 0.72×10^{-3} mm²/s for D (l). DW, diffusion-weighted; D_f , diffusion coefficient of the fast compartment; D_s , diffusion coefficient of the slow compartment; F_f , fraction of the fast compartment; F_s , fraction of the slow compartment; ADC_{LB}, apparent diffusion coefficient at low b -value range; ADC_{HB}, apparent diffusion coefficient at high b -value range; K , diffusional kurtosis; D , corrected diffusion coefficient.

Table 3 FAZA-PET T/M and the DWI parameter estimates

	T/M	D_f ($\times 10^{-3}$ mm ² /s)	D_s ($\times 10^{-3}$ mm ² /s)	F_f	F_s	ADC _{LB} ($\times 10^{-3}$ mm ² /s)	ADC _{HB} ($\times 10^{-3}$ mm ² /s)	K	D ($\times 10^{-3}$ mm ² /s)
Primary tumor	1.82 ± 0.57	1.97 ± 0.38	0.44 ± 0.12	0.46 ± 0.14	0.54 ± 0.14	0.92 ± 0.17	0.42 ± 0.09	0.91 ± 0.24	1.01 ± 0.21
Metastatic lymph node	1.63 ± 0.44	2.11 ± 0.36	0.45 ± 0.09	0.40 ± 0.09	0.60 ± 0.09	0.87 ± 0.15	0.44 ± 0.06	0.95 ± 0.30	0.96 ± 0.19

There is no significant difference between parameter estimates of primary tumor and those of metastatic lymph node. FAZA, ¹⁸F-fluoroazomycin arabinoside; PET, positron emission tomography; T/M, tumor-to-muscle ratio; DWI, diffusion-weighted imaging; D_f , diffusion coefficient of the fast compartment; D_s , diffusion coefficient of the slow compartment; F_f , fraction of the fast compartment; F_s , fraction of the slow compartment; ADC_{LB}, apparent diffusion coefficient at low b -value range; ADC_{HB}, apparent diffusion coefficient at high b -value range; K , diffusional kurtosis; D , corrected diffusion coefficient.

destruction of the cell membrane in hypoxic cells will elevate D_s . There was a significant positive correlation between D_s and FAZA T/M in this study. That is, D_s increased as the tissue oxygenation became lower. However, there was no correlation between F_s and T/M. F_s is reported to increase with an increase of cell diameter, but it also decreases with an increase of cell membrane permeability and destruction

of cell membrane.⁶ The result that there was no significant change in F_s could be due to a combination of the effects above.

Since ADC_{HB} is a value reflecting slowly diffusing molecules, it was anticipated that changes in cell structure could be detected with ADC_{HB}. However, neither ADC_{LB} nor ADC_{HB} were correlated with T/M. From this result, it is concluded that

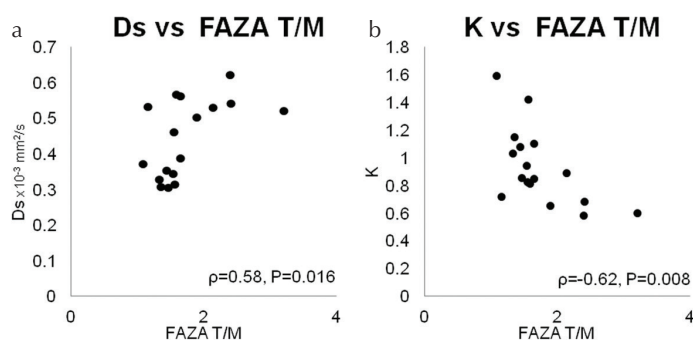


Fig. 2 Scattergrams displaying the relationship between FAZA activity T/M and D_s (a) and K (b). A significant positive correlation was found between D_s and T/M ($\rho = 0.58, P = 0.016$), and a significant negative correlation between K and T/M ($\rho = -0.62, P = 0.008$). FAZA, ¹⁸F-fluoroazomycin arabinoside; T/M, tumor-to-muscle ratio; D_s , diffusion coefficient of the slow compartment; K , diffusional kurtosis.

Table 4 Spearman's rank correlation coefficient between FAZA-PET T/M and the DWI parameter estimates

	D_f	D_s	F_f	F_s	ADC _{LB}	ADC _{HB}	K	D
Spearman's rank correlation coefficient (ρ)	0.24	0.58	-0.18	0.18	0.35	0.34	-0.62	0.23
P	0.35	0.016*	0.49	0.49	0.17	0.19	0.008*	0.37

* $P < 0.05$ is significant. FAZA, ¹⁸F-fluoroazomycin arabinoside; PET, positron emission tomography; T/M, tumor-to-muscle ratio; DWI, diffusion-weighted imaging; D_f , diffusion coefficient of the fast compartment; D_s , diffusion coefficient of the slow compartment; F_f , fraction of the fast compartment; F_s , fraction of the slow compartment; ADC_{LB}, apparent diffusion coefficient at low b -value range; ADC_{HB}, apparent diffusion coefficient at high b -value range; K , diffusional kurtosis; D , corrected diffusion coefficient.

changes in the hypoxic tissue cannot be detected with the ADC, even for the high b -value range.

It has been reported that K increases in tumor as the tissue structure becomes more complex due to the increased cell density and cell size.^{9,12} In this study, K was negatively correlated with T/M, so that it decreased with the tissue oxygenation level. It is thought that the decrease of K can be attributed to the increase in cell membrane permeability and destruction of cell membrane; that is, the decreased complexity of the tissue. An increase in cell diameter might have increased K , but the influence is thought to be small. On the other hand, there was no correlation between D and T/M. D mainly reflects b -value dependent signal change in the low b -value range. Therefore, the trend for D is similar to that for ADC_{LB}, and it is reasonable that neither parameter had a significant correlation with T/M. Unfortunately, because there is no clear biological model for DKI, the mechanism by which the changes in the tissues affect the DKI parameters is uncertain, so further studies will be needed.

There were some limitations in this study. First, the number of subjects was small. One reason for this is that there were several cases where the lesion could not be identified with DWI due to susceptibility or motion artifacts. Also, tumors of different histopathological type were included in the study. Furthermore, all subjects were diagnosed with a malignant tumor after biopsy, and treated with chemoradiotherapy. Therefore, surgical specimens were not obtained, and comparison between histopathological and imaging findings could not be performed. A second limitation was that only the median value of the ROI was used to estimate the

DWI parameters. It is difficult to adequately represent the features of an inhomogeneous tumor with only the median value of the ROI. To use DWI for planning of radiotherapy, such as intensity modulated radiation therapy, pixel-by-pixel evaluation is necessary. In addition, there may be a difference in which pixels were used to obtain the DWI parameter estimates and the FAZA T/M. That is, the DWI ROI may not have contained all of the same pixels as the FAZA-PET ROI, and vice versa. It is possible that such a discrepancy might have affected the results.

Conclusion

A correlation between DWI parameters and FAZA-PET activity was investigated in head and neck carcinoma. The estimate of D_s obtained from a two-compartment model had a significant positive correlation with FAZA-PET activity T/M, and K from DKI had a significant negative correlation, which suggests that those DWI parameters might be useful as indicators for changes in the structure of hypoxic cells.

Funding

This work was supported by grants from KAKENHI (15H04910), and the Japan Advanced Molecular Imaging Program, MEXT, Japan.

Conflicts of Interest

The authors declare that they have no conflicts of interest.

References

1. Hill RP, Bristow RG. The scientific basis of radiotherapy, In: Tannock IF, Hill RP, Bristow RG, Harrington L, eds. *The Basic Science of Oncology*, 4th ed. New York: McGraw-Hill; 2005: 289–321.
2. Lee ST, Scott AM. Hypoxia positron emission tomography imaging with ^{18}F -fluoromisonidazole. *Semin Nucl Med* 2007; 37:451–461.
3. Saga T, Inubushi M, Koizumi M, et al. Prognostic value of PET/CT with ^{18}F -fluoroazomycin arabinoside for patients with head and neck squamous cell carcinomas receiving chemoradiotherapy. *Ann Nucl Med* 2016; 30:217–224.
4. Rischin D, Fisher R, Peters L, Corry J, Hicks R. Hypoxia in head and neck cancer: studies with hypoxic positron emission tomography imaging and hypoxic cytotoxins. *Int J Radiat Oncol Biol Phys* 2007; 69:S61–S63.
5. Kumar V, Abbas AK, Fausto N, Mitchell RN. Cell injury, cell death, and adaptations, In: Kumar V, Abbas AK, Fausto N, Mitchell RN, eds. *Robbins Basic Pathology*. 8th ed. Philadelphia: Elsevier; 2007: 1–30.
6. Obata T, Kershaw J, Tachibana Y, et al. Comparison of diffusion-weighted MRI and anti-Stokes Raman scattering (CARS) measurements of the inter-compartmental exchange-time of water in expression-controlled aquaporin-4 cells. *Sci Rep* 2018; 8:17954.
7. Le Bihan D. The ‘wet mind’: water and functional neuroimaging. *Phys Med Biol* 2007; 52:R57–R90.
8. Jensen JH, Helpert JA, Ramani A, Lu H, Kaczynski K. Diffusional kurtosis imaging: the quantification of non-Gaussian water diffusion by means of magnetic resonance imaging. *Magn Reson Med* 2005; 53:1432–1440.
9. Jensen JH, Helpert JA. MRI quantification of non-Gaussian water diffusion by kurtosis analysis. *NMR Biomed* 2010; 23:698–710.
10. Urushihata T, Takawa H, Seki C, et al. Water diffusion in the brain of chronic hypoperfusion model mice: a study considering the effect of blood flow. *Magn Reson Med Sci* 2018; 17:318–324.
11. Piert M, Machulla HJ, Picchio M, et al. Hypoxia-specific tumor imaging with ^{18}F -fluoroazomycin arabinoside. *J Nucl Med* 2005; 46:106–113.
12. Hori M, Fukunaga I, Masutani Y, et al. Visualizing non-Gaussian diffusion: clinical application of q-space imaging and diffusional kurtosis imaging of the brain and spine. *Magn Reson Med Sci* 2012; 11:221–233.